CORROSION 2018, 74:276–287.

Effects of CO_2 and H_2S on Corrosion of Martensitic Steels in Brines at Low Temperature

Ruishu Feng,[§,,**,***] Justin R. Beck,[§,*,**] Derek M. Hall,[*,**] Aysel Buyuksagis,[**] Margaret Ziomek-Moroz,[‡,****] and Serguei N. Lvov[‡,*,**,*****]*

ABSTRACT

Corrosion studies were conducted for martensitic carbon steels in 5 wt% NaCl brine solutions at 4°C and 10 MPa (1,450 psi). These studies simulated different subsurface environments relevant to Arctic drilling. Here, two high-strength martensitic carbon steels, S-135 and UD-165, were studied in three different environments: (1) a CO_2-NaCl-H_2O solution with a CO_2:H_2O molar ratio of 0.312 in the whole system, (2) an H_2S-NaCl-H_2O solution with an H_2S:H_2O molar ratio of 3.12×10^{-4}, and (3) a CO_2-H_2S-NaCl-H_2O solution with the same acid gas to water ratios as environments 1 and 2. Results from the CO_2+H_2S mixed environment indicated that sour corrosion mechanism was dominant when the CO_2:H_2S molar ratio was 1,000. This impact of a small amount of H_2S on the corrosion mechanism could be attributed to the specific adsorption of H_2S on the steel surface. Electrochemical and mass loss measurements showed a distinct drop in the corrosion rate (CR) by more than one order of magnitude when transitioning from sweet to sour corrosion. This inhibiting effect on CR was attributed to the formation of a protective sulfide thin film. Tafel analyses of the anodic reaction showed that the Bockris mechanism was unlikely in the conditions tested. When comparisons were made between modeled and experimental CRs, good agreement was found in the CO_2-only and H_2S-only environments, but not in the CO_2+H_2S environment.

KEY WORDS: cold-climate corrosion, corrosion mechanism, corrosion rate, martensitic carbon steels, sweet and sour corrosion

Submitted for publication: January 31, 2017. Revised and accepted: October 5, 2017. Preprint available online: October 5, 2017, https://doi.org/10.5006/2406.

‡ Corresponding authors. E-mail: lvov@psu.edu (S.N. Lvov), Margaret.Ziomek-Moroz@netl.doe.gov (M. Ziomek-Moroz).
§ First authors.
* Department of Energy and Mineral Engineering, The Pennsylvania State University, University Park, PA 16802.
** The EMS Energy Institute, The Pennsylvania State University, University Park, PA 16802.
*** Current address: U.S. Department of Energy, National Energy Technology Laboratory, Pittsburgh, PA 15236.
**** U.S. Department of Energy, National Energy Technology Laboratory, 1450 Queen Avenue SW, Albany, OR 97321.
***** Department of Materials Science and Engineering, The Pennsylvania State University, University Park, PA 16802.

INTRODUCTION

The effects of CO_2 and H_2S on corrosion processes are of considerable interest to the oil and gas industry for a number of reasons.[1-10] Though the individual impacts of each gas are fairly well agreed on, more understanding is still needed for mixed cases and extreme conditions. In the case of sweet corrosion (CO_2 corrosion), it is well known that dissolved CO_2 lowers the solution pH and increases the rate of corrosion.[11-14] As for sour corrosion (H_2S corrosion), the presence of H_2S in low concentrations typically decreases the corrosion rate (CR).[15-19] The proposed mechanism for the CR drop associated with H_2S is the formation of a protective iron sulfide film. However, while this reduced CR may be preferred in some cases, the tradeoff is that sulfide stress cracking becomes a possibility. With different failure modes being possible between CO_2 and H_2S corrosion, it is particularly important to understand when corrosion behaviors change for systems with these two acid gases. As the conditions for transition between sweet and sour corrosion are still

ISSN 0010-9312 (print), 1938-159X (online)
18/000045/$5.00+$0.50/0

poorly defined, a better understanding is critical for applications such as corrosion prevention and mitigation where both components are present.

Currently, no widespread law or model exists for determining the transition between sweet and sour corrosion. Though NACE SP0110 Appendix A provides a rough rule for determining the sweet-sour transition,[20] a number of studies have provided evidence that this approach may be flawed in some cases. This guideline states that a molar ratio of CO_2:H_2S above 500 would be expected to produce sweet corrosion, whereas a ratio below 20 would lead to sour corrosion. A ratio between 20 and 500 could display mixed corrosion mechanisms. However, Smith investigated the assumption of 500 on the upper end of the CO_2:H_2S ratio.[21] Although thermodynamic calculations for the stability of corrosion products could justify the transition point of 500, the stability of corrosion products was extremely sensitive to the quality of the thermodynamic data used, and moderately sensitive to temperature and solution ionic strength. As an example, 1% change in the Gibbs free energy value for $FeCO_3$ could change the sweet-sour corrosion transition point by more than a factor of 10.

In addition to the uncertainty identified by Smith, laboratory experiments have been investigating the kinetic effects of different CO_2:H_2S ratios over a wide range of conditions. These results have shown that CO_2:H_2S ratios from 500 to as high as 10,000 can still see a decrease in CR associated with sour corrosion.[15-19] As such, more experimental evidence is needed to better clarify the sweet-sour corrosion transition. These concerns are especially relevant to cold-climate corrosion in Arctic drilling projects. Although the temperatures are lower, there is a possibility of higher corrosion risk resulting from higher concentrations of dissolved acid gases in deep wells.[22-23]

The purpose of this work was to provide data and discussion on the effects of CO_2 and H_2S in simulated Arctic environments. Corrosion properties of two different martensitic carbon steels were investigated using electrochemical techniques, mass loss measurements, software modeling, and surface analyses. The resulting data provided some insights into the influence of CO_2:H_2S ratio on sweet-sour corrosion transition when the temperature was low.

EXPERIMENTAL

Test Conditions

A temperature of 4°C was selected with a total system pressure of 10 MPa. The test solution contained 5 wt% NaCl (0.9 mol/kg). The sweet, sour, and mixed conditions were prepared by holding the test solution in equilibrium with different non-aqueous phases. The three cases used were: (1) CO_2, (2) an H_2S/Ar mixture, and (3) a CO_2/H_2S/Ar mixture. It should be noted that CO_2 is a liquid phase at 10 MPa and 4°C.[24] The formation of CO_2 hydrate was also possible at the interface between liquid CO_2 and the aqueous phase.[25-26] However, its impact on corrosion was not considered in this work because corrosion was mostly determined by the bulk aqueous solution. Care should be taken to describe the system at high pressures when referring to such substances as "gas" or "vapor" phases. Therefore, inputs were described using molar fractions as opposed to partial pressures.

Test procedures were designed to allow consistent dosing of substances to reach the desired molar fractions. Deep wells are predicted to encounter total pressures up to 100 MPa, and the "gas" phase may contain over 10% CO_2 and 0.01% H_2S.[9] Here, experimental conditions were calculated to represent exposures with a similar ratio. The total amount of each component in all of the phases was calculated, and the system was defined using the X:H_2O molar ratios, where X represents the non-water species such as NaCl, CO_2, H_2S, and Ar. The molar ratios used for laboratory testing were CO_2:H_2O = 0.312 and H_2S:H_2O = 3.12×10^{-4}. These two fractions maintained a ratio of CO_2:H_2S = 1,000:1 for the mixed case when mixed. The Ar:H_2O ratio was not controlled, but rather Ar was used to balance the total pressure between tests. Phase equilibria calculations were performed using commercial thermodynamic modeling software (OLI Analyzer[†]) to determine the amounts of each species needed to achieve the internal autoclave volume (476 mL after assembly) at 4°C and a total pressure of 10 MPa. System compositions (in mol) for the three test environments are given in Table 1. To achieve the total pressure, the amounts of H_2O and H_2S were higher in the H_2S-only condition than in the CO_2-containing conditions, while the molar ratios were the same.

Electrode Materials

Two different martensitic drilling steels were tested: a high-strength low-alloy carbon steel commonly used for drill pipe, grade S-135, and a newly designed ultra-high-strength low-alloy carbon steel, grade UD-165. Their chemical compositions are given in Table 2.[27] UD-165 has lower chromium, but higher nickel, copper, and sulfur than S-135.

CRs were quantified from working electrodes and mass loss samples. To electrochemically quantify the CR, working electrodes with dimensions of 10 mm × 10 mm × 5 mm were prepared out of each material. Only

TABLE 1
Test Conditions for Corrosion Tests (mol) at 4°C

	H_2S	CO_2	H_2O	NaCl	Ar
CO_2	0	4.52	14.49	0.235	0
CO_2+H_2S	4.49×10^{-3}	4.49	14.40	0.233	0.0404
H_2S	6.30×10^{-3}	0	20.20	0.327	0.5597

[†] Trade name.

TABLE 2
Chemical Compositions (mass%) of S-135 and UD-165

Steel	Fe	Cr	Mn	Mo	Al	Ni	Cu	Nb	S
S-135	Bal.	1.39	0.78	0.68	0.03	0.02	0.02	<0.01	0.002
UD-165	Bal.	0.79	0.88	0.67	0.03	0.81	0.19	0.02	0.007

Steel	P	B	C	N	V	Si	Sn	Ti
S-135	0.006	<0.005	0.26	0.005	<0.01	0.3	<0.01	<0.01
UD-165	<0.005	<0.005	0.27	0.007	0.07	0.26	<0.01	<0.01

one 10 mm × 10 mm face of each working electrode was exposed to the test solution, and all other sides were coated with an epoxy. A Type 304 stainless steel (UNS S30400[1]) wire was attached to the opposite 10 mm × 10 mm face as the electrical lead. The wire was coated with shrinkable polytetrafluoroethylene (PTFE) tubing to avoid any unwanted galvanic couples. Three working electrodes of the same steel were sealed into a PTFE holder using the epoxy. Mass loss samples were prepared using 25 mm × 20 mm × 2 mm plates. A hole with 3 mm internal diameter was drilled near the top of each plate so that the samples could be suspended from a PTFE-coated wire. The working electrode surfaces and the mass loss samples were both sanded with 600 grit SiC paper and then cleaned in acetone inside an ultrasonic bath for 30 min to 60 min.

System Setup

All measurements were performed in a 600 mL autoclave (Parr 4560†). A PTFE liner was used to isolate the test solution from the autoclave vessel. The custom three-electrode assemblies and the mass loss samples were submerged in the test solutions within the autoclave. Temperature was controlled using a circulating chiller and a copper coil cooling loop wrapped around the autoclave vessel. Pressure was monitored with a mounted pressure transducer in the lid. All of the test systems were stirred using an impeller rotating at 150 revolution per minute (rpm). A computer-controlled Gamry Reference 600† potentiostat was used to perform the electrochemical measurements.

Within the autoclave, electrochemical measurements were performed using the three-electrode approach. The working electrodes were the steel samples to be studied. The counter electrodes were 20 mm × 10 mm × 1 mm platinum plates or meshes. Electrode leads were all coated with shrinkable PTFE. To place each counter electrode parallel to a corresponding working electrode in the system, counter electrode leads were inserted through the electrode assembly edge. A schematic of the autoclave system is shown in Figure 1.

Custom double-junction Ag/AgCl reference electrodes were used as reference electrodes. The filling solution was 5 wt% NaCl to minimize any liquid junction potential between the reference electrode and test solutions. The inner junction of the reference electrode consisted of the Ag/AgCl electrode submerged in solution-saturated zirconia sand inside an alumina ceramic tube. The top of the tube was sealed with an epoxy, and the bottom was supported using a porous zirconia-magnesia cement. The second junction was prepared by sealing a shrinkable PTFE tube around the outside of the ceramic tube. Inside this extended PTFE tube was filled again with solution-saturated zirconia sand, and either another cement frit or a perforated PTFE plug was used to support the second junction. Two reference electrodes were used in each test. New electrodes were prepared for each experiment. The reference electrode potential at 4°C

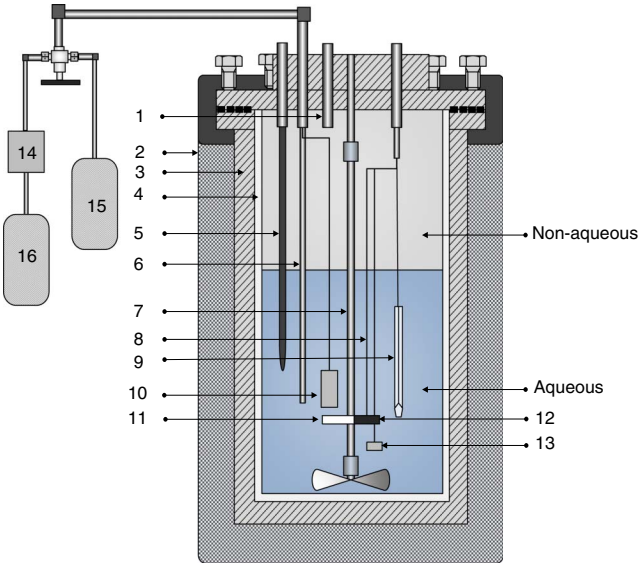

FIGURE 1. *Schematic diagram of the autoclave system. 1: Connection to pressure transducer. 2: Copper coil cooling loop. 3: Autoclave stainless steel vessel. 4: PTFE liner. 5: Polymer-coated thermocouple. 6: Dip tubing. 7: Epoxy-coated stirrer. 8: PTFE-coated working electrode leads. 9: Two Ag/AgCl reference electrodes. 10: Two mass loss samples. 11: PTFE sample holder assembly. 12: Three steel working electrodes. 13: Three Pt counter electrodes. 14: Supercritical CO_2 pump. 15: H_2S/Ar cylinder or Ar cylinder. 16: CO_2 cylinder.*

[1] UNS numbers are listed in *Metals and Alloys in the Unified Numbering System*, published by the Society of Automotive Engineers (SAE International) and cosponsored by ASTM International.

was calculated to be 0.248 V vs. the standard hydrogen electrode (SHE) using the data from the thermodynamic modeling software. The results were confirmed through comparison with calculations performed using thermodynamic properties and activity coefficients from literature.[28-30]

Each test used a total of three working electrodes and two mass loss samples that would be simultaneously exposed to the same test solution. Only one steel (either S-135 or UD-165) was studied during each test. Data collected from these samples were used to calculate the average and standard deviation (SD) values for each material.

Experimental Procedures

To achieve the desired system pressure and chemical compositions shown in Table 1, an experimental procedure was developed. First, the electrode assemblies and mass loss samples were added to the autoclave. The desired amount of dry NaCl was placed at the PTFE liner bottom before the autoclave was sealed. After sealing, oxygen was purged from the system by repeatedly pressurizing with Ar (ultra high purity) to 2 MPa (290 psi) then depressurizing to ambient. During the pressure cycles, the system was cooled to 4°C. The system was allowed to chill overnight to ensure a stable temperature (±1°C) for gas injection.

Next, H_2S was added (when applicable) using a 10 vol% H_2S in Ar blend through the dip tubing (number 6 in Figure 1). The H_2S/Ar blend was used for safety reasons. The desired pressure of H_2S/Ar blend was calculated using the available internal volume left in the autoclave (476 mL). In the H_2S-only condition, a certain amount of Ar was added so that the final addition of water could reach the desired system pressure and H_2S:H_2O molar ratio.

After the addition of any H_2S required, water was injected into the system. Water was deionized (DI) using a Milli-Q† system to a resistivity of 18 MΩ·cm. The DI water was then deaerated with Ar through a sparger for at least 1 h prior to injection. The deaerated DI water was injected into the system using a high performance liquid chromatography (HPLC) pump. The HPLC pump was set at a flow rate of 10 mL/min and run until the desired amount of water was transferred to the system. For the H_2S-only system, water injection was the final step. It should be noted that while the target pressure was 10 MPa, the actual pressure was in the range of 7 MPa to 8 MPa in the H_2S-only case. This was likely the result of uncertainty in measuring the autoclave internal volume and uncertainties in thermodynamic values used to determine the amount of mass needed to reach the desired pressure. Nevertheless, the molar ratio of H_2S:H_2O was consistent with the other conditions.

For the cases requiring CO_2, 99.99% purity CO_2 was added using a supercritical CO_2 pump directly after water injection to achieve and maintain the total pressure of 10 MPa.

Once the desired conditions were reached, electrochemical measurements were performed. Linear polarization resistance (LPR) and electrochemical impedance spectroscopy (EIS) measurements over time were used to determine when the system approached a steady state. The CRs over time in Figure 2 indicate that the system approached the steady state by the 60 h mark. After 60 h, cyclic voltammetry (CV) and linear sweep voltammetry (LSV) were used, in addition to LPR and EIS, to study electrochemical properties of the working electrodes. LPR was measured at a scan rate of 0.1 mV/s over a range of ±15 mV around the corrosion potential, E_{corr}. EIS was performed with an amplitude of 10 mV over a frequency range from

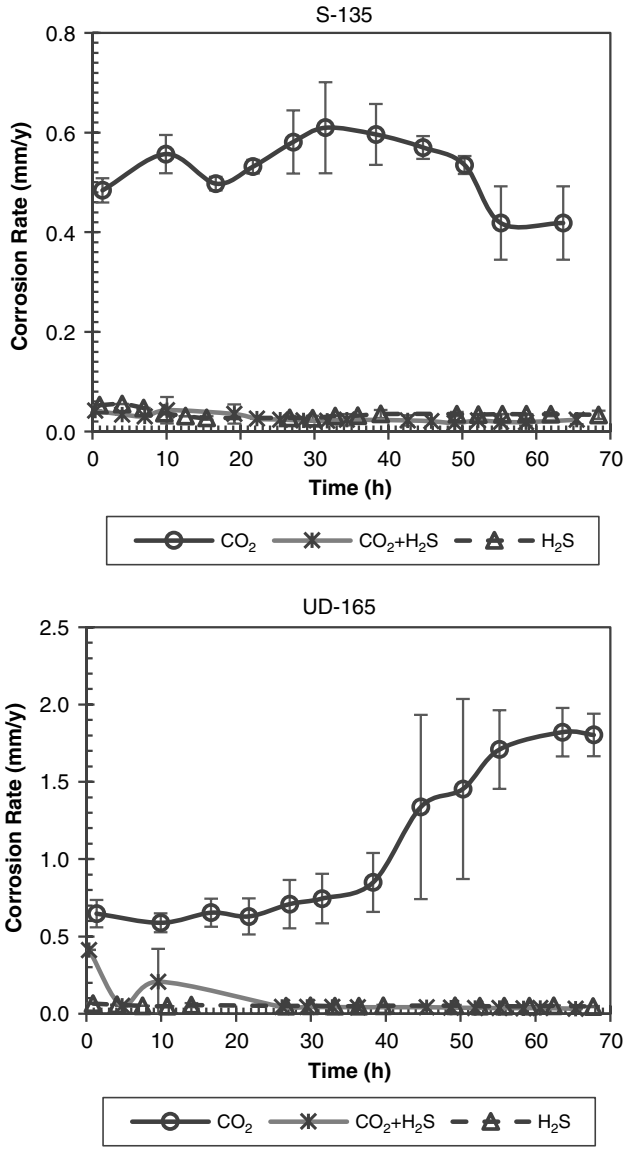

FIGURE 2. *Corrosion rates from LPR for S-135 (top) and UD-165 (bottom) with SD over time in the CO_2-only, CO_2+H_2S, and H_2S-only cases. Conditions: 4°C, 0.9 mol/kg NaCl solutions, 150 rpm.*

TABLE 3

The Calculated pH and Carbonate and Sulfide Species in the Aqueous Phase (mol/kg H_2O)

Time (t)	0			60 h (UD-165)		
Conditions	**CO_2**	**CO_2+H_2S**	**H_2S**	**CO_2**	**CO_2+H_2S**	**H_2S**
pH	3.0	3.0	4.5	4.2	3.4	5.5
CO_2(aq)	1.43	1.44	0	1.40	1.41	0
HCO_3^-(aq)	9.29×10^{-4}	9.28×10^{-4}	0	1.99×10^{-2}	2.63×10^{-3}	0
CO_3^{2-}(aq)	1.48×10^{-10}	1.47×10^{-10}	0	5.89×10^{-8}	1.01×10^{-9}	0
H_2S(aq)	0	3.29×10^{-3}	1.41×10^{-2}	0	3.25×10^{-3}	1.35×10^{-2}
HS^- (aq)	0	2.12×10^{-7}	3.39×10^{-5}	0	5.08×10^{-7}	3.60×10^{-4}
S^{2-}(aq)	0	1.68×10^{-19}	7.75×10^{-16}	0	9.70×10^{-19}	9.14×10^{-14}

200 kHz down to 5 mHz. After the system reached the steady state, CV was run at a sweep rate of 50 mV/s. LSV was conducted at a scan rate of 1 mV/s, sweeping up and down from E_{corr}. One of the three working electrodes in each test was used for surface analysis, so it was not polarized with CV and LSV. The CV and LSV were only run in the two 1×1 cm^2 working electrodes, and the dissolved Fe resulting from polarization was of the order of 10^{-6} mol, which was negligible compared to the Fe dissolution over 60 h. All of the direct current (DC) curves were corrected to take into account the solution resistance (R_{sol}) measured from EIS. Total exposure time was recorded for mass loss calculation (90 h to 120 h).

After each test was completed, the autoclave system was depressurized and then disassembled. All electrodes and mass loss samples were rinsed with distilled water, dried with Ar, and then sealed in sample bags under Ar. The working electrode used for surface analysis was examined with scanning electron microscopy (SEM) and energy dispersive x-ray spectroscopy (EDS). Mass loss samples were cleaned and analyzed according to ASTM G1-03 using Solution C.3.5 (HCl and hexamethylene tetramine) as described in Appendix A1.[31] Polished and unexposed samples were also cleaned to serve as calibrations for material loss resulting from the cleaning procedure.

RESULTS AND DISCUSSION

Solution Speciation

The thermodynamic calculation showed that CO_2(aq) and H_2S(aq) were the dominant carbonate and sulfide aqueous species in the conditions tested. The speciation was calculated using a commercial thermodynamic modeling software.[32] The calculated pH, carbonate species, and sulfide species are given in Table 3. Note that concentrations in the aqueous phase are expressed in mol/kg H_2O. Before corrosion took place, the solution pH was 3.0 for the CO_2-containing conditions, whereas it was 4.5 for the H_2S-H_2O-NaCl condition. For the CO_2-containing conditions, CO_2(aq) was the dominant carbonate species dissolved in the aqueous phase. For the mixed CO_2+H_2S condition, the H_2S(aq) concentration was calculated to be lower than CO_2(aq) by three orders of magnitude, which barely changed the pH and carbonate speciation compared with the CO_2-only case. For the H_2S-only condition, H_2S(aq) was the dominant sulfide species.

In the CO_2+H_2S condition, the H_2S(aq) concentration was smaller than in the H_2S-only condition by a factor of 4. This was a result of the dissolution of H_2S in the CO_2 liquid phase, which was calculated to be 1.40×10^{-2} mol/kg H_2O. This value was converted to the mol/kg H_2O scale for the sake of comparison. Therefore, the molar ratio of CO_2:H_2S = 1,000:1 in the whole system (aqueous and non-aqueous phases) resulted in an aqueous CO_2(aq):H_2S(aq) ratio of approximately 440.

The solution pH increased after 60 h of corrosion process, as shown in Tables 3 and 8. The pH and speciation were calculated taking account of Fe dissolution, and the dissolved Fe was calculated over 60 h using Faraday's law of electrolysis. The largest increase in pH was 1.2 in the CO_2-only condition for UD-165. Although the pH increase corresponded to some speciation change, the dominant carbonate and sulfide species remained as CO_2(aq) and H_2S(aq). The aqueous CO_2(aq):H_2S(aq) ratio was still close to 440 in the CO_2+H_2S condition.

Polarization Resistance and Corrosion Rate

Both steels showed a correlation between R_{pol} and the presence of H_2S. Steady-state polarization resistances, R_{pol}, of S-135 and UD-165 are listed in Table 4. R_{pol} increased by more than one order of magnitude in the presence of H_2S, indicating that a

TABLE 4

Polarization Resistance R_{pol} ($\Omega\cdot cm^2$) Results for S-135 and UD-165 After 60 Hours

Steel	Gas	LPR	EIS
S-135	CO_2	336±59	326±46
	CO_2+H_2S	8,067±3,048	8,236±3,213
	H_2S	4,038±483	4,013±566
UD-165	CO_2	76±7	95±18
	CO_2+H_2S	4,180±526	4,286±711
	H_2S	2,722±184	2,702±206

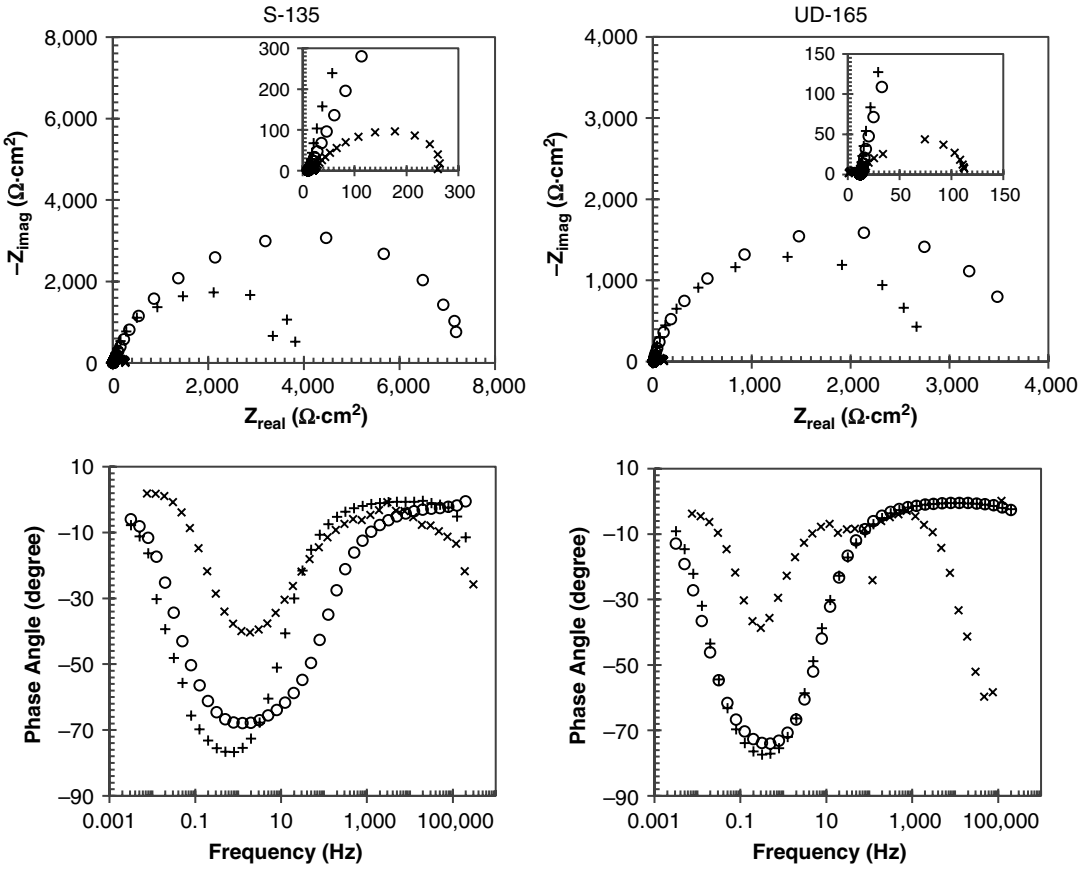

FIGURE 3. *Nyquist plots and Bode phase angle plots for S-135 (left) and UD-165 (right) after 60 h. Conditions: 4°C, 0.9 mol/kg NaCl solutions, 150 rpm. Symbols: x = CO_2, o = CO_2+H_2S, + = H_2S.*

small amount of H_2S decreased corrosion on these steels at 4°C. This matched the behavior that has been reported for low concentrations of H_2S at other temperatures.[19,33] For each steel, R_{pol} in the H_2S-only case was about half of that in the CO_2+H_2S condition. This indicates that although the H_2S presence decreased corrosion compared to CO_2, a higher H_2S(aq) concentration increased corrosion compared to the lower concentration of H_2S(aq).

The EIS results confirmed the active corrosion behavior, which was one assumption used to calculate the CR.[30,34] The representative Nyquist plots and Bode phase angle plots at steady sate are shown in Figure 3. The Nyquist plots were depressed semicircles with one time constant. The phase angles in the CO_2+H_2S condition were determined by H_2S instead of CO_2. The data were fitted using the Randles circuit without diffusion, shown in Figure 4. R_{sol} represents the solution resistance, and R_{pol} represents the polarization resistance. A constant phase element (CPE) was used to account for non-ideality of the double-layer capacitance, C_{dl}.

The CRs of S-135 and UD-165 were calculated according to the Stern-Geary equation using R_{pol}.[2,34] The Tafel slopes were calculated assuming the symmetry coefficient (β) was 0.5 and two electrons were transferred in the Fe dissolution reaction, following Equations (2) and (8). In Figure 2, the CRs over time fluctuated at the early stage and then approached a steady state by 60 h. The CRs from LPR, EIS, and mass loss samples after 60 h are given in Table 5. Inversely with R_{pol}, the CR dropped by more than one order of magnitude in the presence of H_2S.

In Table 5, CRs from LPR and EIS were all within a few percentages of one another. When comparing CRs from electrochemical and mass loss measurements, results were generally within 30% for the CO_2-only case, which was fairly close considering the SDs. But for the H_2S-containing cases, CRs from mass loss samples were almost three times larger than those from electrochemical tests. The difference was attributed to relatively larger errors in the mass loss

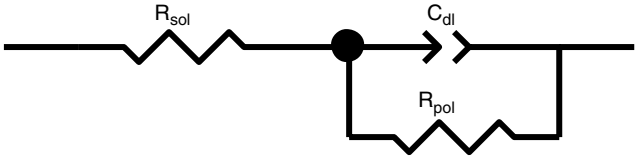

FIGURE 4. *Equivalent circuit used to fit EIS data.*

TABLE 5

Corrosion Rate (mm/y) Results for S-135 and UD-165 After 60 Hours

Steel	Gas	LPR	EIS	Mass Loss	Modeled, t = 60 h
S-135	CO_2	0.42±0.07	0.43±0.06	0.59±0.02	2.42
	CO_2+H_2S	0.019±0.007	0.019±0.008	0.060±0.015	2.50
	H_2S	0.035±0.004	0.035±0.005	0.080±0.014	0.049
UD-165	CO_2	1.8±0.2	1.5±0.3	1.8±0.3	2.21
	CO_2+H_2S	0.033±0.004	0.033±0.005	0.088±0.004	2.96
	H_2S	0.051±0.004	0.052±0.004	0.068±0.024	0.049

measurements when the CR was lower. It was found that the material lost from each exposure to the cleaning solution was of a similar order to the mass lost from corrosion in H_2S-containing conditions, which likely resulted in exaggerated CRs.

In all three conditions, UD-165 had higher CRs than S-135. The CR was higher by a factor of two in the presence of H_2S and a factor of four without H_2S. The higher CR of UD-165 may originate from its chemical composition and microstructure.

Overall, it can be seen that a molar ratio of CO_2:H_2S as high as 1,000 was still enough to transition from sweet to sour corrosion in the low-temperature and high-pressure environment tested here. Furthermore, the ratio of dissolved CO_2(aq):H_2S(aq) may present a more convenient approach to estimating sweet to sour corrosion transition points. The CRs obtained indicate that sour corrosion was still dominant at aqueous CO_2(aq):H_2S(aq) ratio around 440 in the low-temperature regime.

Cyclic Voltammetry Results

From CV curves, two observations were made at the low-temperature conditions. (1) No obvious limiting currents were observed in the anodic region, indicating that all anodic reactions showed no clear signs of mass transport limitations. This result agreed with the reported effects of CO_2 and H_2S in literature.[17,35-38] (2) A peak was observed in the anodic sweep for systems with H_2S but was absent without H_2S. As such, sulfide-related electrochemical reactions did contribute to corrosion polarization curves even in the case with a high CO_2:H_2S ratio. Representative CV curves for the two steels are shown in Figure 5.

Tafel Analysis

A Tafel analysis of LSV data showed an observable impact of H_2S on both anodic and cathodic Tafel slopes compared to those obtained without H_2S. Representative LSV plots for each steel are shown in Figure 6. The anodic (b_a) and cathodic (b_c) Tafel slopes were taken at least 50 mV from E_{corr}. The average Tafel slopes were obtained from two working electrodes and are given in Table 6 along with SDs.

The Tafel slopes (b_a or b_c) from S-135 were within 1 SD between the two cases containing H_2S, but significantly different from the CO_2-only case. The Tafel values obtained for UD-165 followed the same trend as S-135 when comparing between different gas cases. These observations fortify the theory that H_2S impacted the corrosion mechanism even when its concentration was significantly lower than CO_2. This impact of a small amount of H_2S on the corrosion mechanism could be attributed to the specific adsorption of H_2S on the steel surface.[39] Additionally, in Figure 6, the largely polarized anodic region (>150 mV vs. E_{corr}) of UD-165 in the CO_2+H_2S condition showed

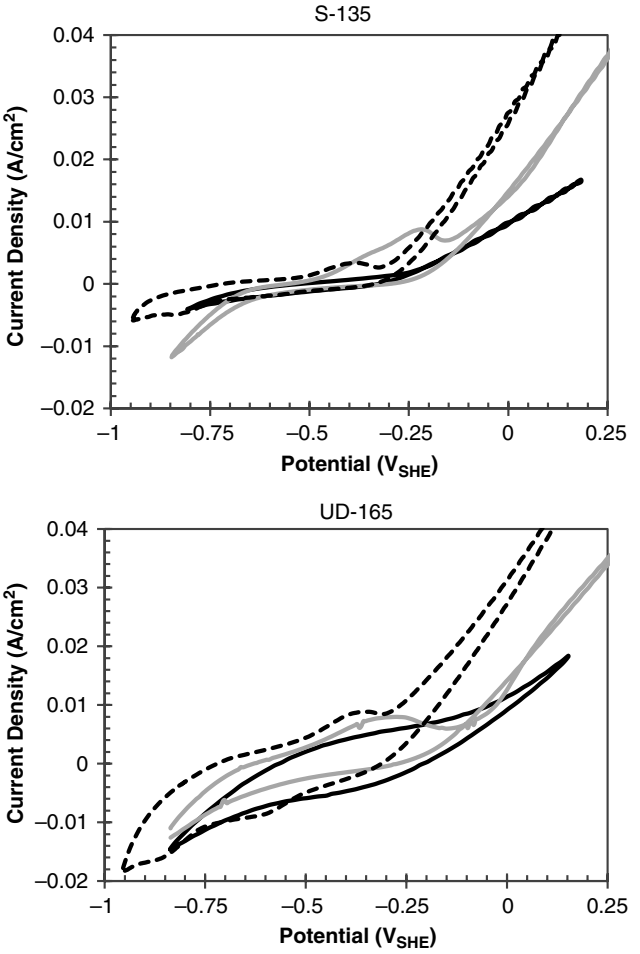

FIGURE 5. *Cyclic voltammetry curves for S-135 (top) and UD-165 (bottom) at 50 mV/s. Conditions: 4°C, 0.9 mol/kg NaCl solutions, 150 rpm. Black = CO_2, gray = CO_2 + H_2S, dashed = H_2S.*

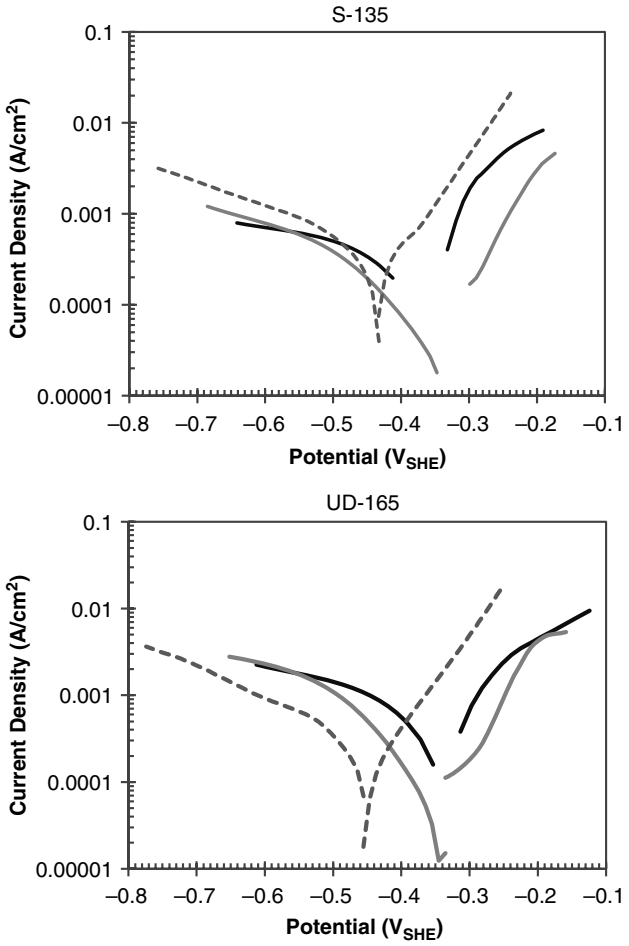

FIGURE 6. *LSV plots for S-135 (top) and UD-165 (bottom) at a scan rate of 1 mV/s. Conditions: 4°C, 0.9 mol/kg NaCl solutions, 150 rpm. Black = CO_2, gray = CO_2+H_2S, dashed = H_2S.*

TABLE 6
The Measured Tafel Slopes (V/decade) for S-135 and UD-165 After 60 Hours

	S-135		UD-165	
Gas	**b_a**	**b_c**	**b_a**	**b_c**
CO_2	0.178±0.024	−0.755±0.000	0.251±0.057	−0.608±0.077
CO_2+H_2S	0.073±0.001	−0.395±0.064	0.063	−0.481
H_2S	0.076±0.021	−0.312±0.098	0.092±0.001	−0.251±0.041

a slope getting close to the anodic Tafel slope in the CO_2-only condition. This slope transition could be explained by the consumption of adsorbed H_2S at the surface and the transition to CO_2 corrosion, if one assumes a layer of H_2S was adsorbed to the surface.

For sweet and sour corrosion processes, a few different mechanisms with Tafel slope values have been proposed. For sour corrosion, Shoesmith, et al.,[40] proposed a chemisorption-oxidation mechanism between Fe and H_2S to form mackinawite in saturated H_2S solutions at 21°C. Ma, et al.,[41] proposed a similar mechanism with two consecutive electron transfers. These two mechanisms are both analogous to the Fe dissolution reaction mechanism proposed by Bockris, et al.,[42] involving an intermediate formation with OH^-(aq). Iofa, et al.,[39] and Zhang, et al.,[7] described a mechanism involving a chemisorbed hydrogen sulfide layer and two electrons transferred simultaneously. For CO_2 corrosion, the anodic mechanism has been frequently assumed to follow the Bockris mechanism, which could well explain some experimental Tafel slopes from 0.03 V/decade to 0.04 V/decade.[8,14,43-44]

Anodic Tafel Analysis — By calculating possible symmetry coefficients from different anodic Tafel slope equations, some observations were made. The anodic Tafel slope equation of the Bockris mechanism is as follows:[42]

$$b_a = \frac{2.303RT}{(1+\beta)F} \quad (1)$$

where R is the gas constant, T is the absolute temperature, and F is the Faraday constant.

In some sweet corrosion studies, Nešić, et al.,[35] reported that b_a values changed from 0.03 V/decade to 0.12 V/decade when pH increased from 4 to 5 at 22°C, indicating a mechanism transition. Videm and Koren stated that the anodic Tafel slope was 0.03 V/decade in the lower polarization region and 0.12 V/decade in the higher polarization region at 25°C.[12] However, the lower polarization regions which gave Tafel slopes of 0.03 V/decade to 0.04 V/decade were found to be so close to the open-circuit potential that they may have been interfered with by the cathodic behavior. Therefore, the b_a value of 0.12 V/decade in the higher polarization region was likely to be the real Tafel slope. b_a of 0.12 V/decade could be correlated with a mechanism involving one electron transferred (n = 1) in the rate determining step (RDS) when assuming the symmetry coefficient (β) to be 0.5 in Equation (2).

$$b_a = \frac{2.303RT}{n(1-\beta)F} \quad (2)$$

where n is the number of electrons transferred in the reaction. It has been proposed by the authors previously that the HCO_3^-(aq) reaction followed the one-electron mechanism at 85°C, and the OH^-(aq) reaction followed the Bockris mechanism at higher pH.[2]

Because of its physical meaning, β should be between 0 and 1, and β is usually assumed as 0.5 for kinetics calculations. To check the applicability of different mechanisms at 4°C, the β values were calculated from the experimental Tafel slopes following different mechanisms to check if β was between 0 and 1. Three anodic reaction mechanisms were considered here: the Bockris mechanism, the one-electron mechanism (1e), and the two-electron mechanism (2e). The calculated β values are given in Table 7.

TABLE 7
Symmetry Coefficients (β) Calculated from the Measured Tafel Slopes

	S-135			UD-165		
Anodic Reaction	**Bockris**	**1e**	**2e**	**Bockris**	**1e**	**2e**
CO_2	–0.69	0.69	0.85	–0.78	0.78	0.89
CO_2+H_2S	–0.25	0.25	0.63	–0.13	0.13	0.57
H_2S	–0.28	0.28	0.64	–0.40	0.40	0.70
Cathodic Reaction	**V-H**	**V-T**	**2e**	**V-H**	**V-T**	**2e**
CO_2	0.07	—	0.04	0.09	—	0.05
CO_2+H_2S	0.14	—	0.07	0.11	—	0.06
H_2S	0.18	—	0.09	0.22	—	0.11

For the anodic reaction in the tested conditions at 4°C, the Bockris mechanism was not possible because its corresponding β values were negative, as shown in Table 7. The corresponding β values were between 0 and 1 for the 1e mechanism and the 2e mechanism. Therefore, neither 1e nor 2e mechanisms could be excluded for any of the conditions tested at 4°C. If both S-135 and UD-165 followed a 1e mechanism for sweet corrosion, a mechanism that produced β values closer to 0.5 than the 2e mechanism, the anodic reaction mechanism for CO_2(aq) could be described by Reactions (3) through (5).

A 1e mechanism for sweet corrosion at low temperatures can be described as:

$$Fe(s)+H_2CO_3(aq)\rightarrow FeHCO_3(ad)+H^+(aq)+e^-(RDS) \quad (3)$$

$$FeHCO_3(ad) \leftrightarrow FeHCO_3^+(ad)+e^- \quad (4)$$

$$FeHCO_3^+(ad)+H^+(aq) \leftrightarrow Fe^{2+}(aq)+H_2CO_3(aq) \quad (5)$$

Unlike the case without H_2S, cases with H_2S provided Tafel slopes that resulted in β values closer to 0.5 when using the equation for the 2e mechanism. The 2e mechanism agreed with the anodic Tafel slopes reported in literature for H_2S-containing solutions, 0.04 V/decade to 0.05 V/decade at 20°C to 30°C, where β would be around 0.6.[38,45-46] However, the International Union of Pure and Applied Chemistry (IUPAC) recommended in 2014 that the simultaneous transfer of more than one electron was highly improbable.[47] Another possibility is that sour corrosion also followed a 1e mechanism but β values were less than 0.5. Given the lack of data available, further evidence is needed to better identify the true elementary reaction steps for the anodic electrochemical reaction during sour corrosion.

Cathodic Tafel Analysis — A similar approach to anodic Tafel analysis was used to study the cathodic Tafel slopes collected for sweet and sour corrosion. Again some possible mechanisms are presented for the cathodic reaction in sweet and sour corrosion. For each mechanism, a Tafel slope equation is presented and corresponding symmetry coefficients were calculated.

For corrosion processes in deaerated solutions, the hydrogen evolution reaction (HER) is commonly assumed to be a primary cathodic reaction. In acidic solutions, the reduction reaction of H^+(aq) is assumed to be the dominant pathway for producing H_2. For the acidic regime, the Volmer-Heyrovsky (V-H) and Volmer-Tafel (V-T) mechanisms are two proposed HER mechanisms. Their Tafel slopes can be calculated using Equations (6) and (7), respectively.[2,48]

Cathodic Tafel slope in the V-H mechanism:[48]

$$b_c = -\frac{2.303RT}{\beta F} \quad (6)$$

Cathodic Tafel slope in the V-T mechanism:[48]

$$b_c = -\frac{2.303RT}{2F} \quad (7)$$

However, dissolved CO_2 and H_2S form weak acids in water and have been proposed to provide alternative mechanisms for hydrogen evolution. One way is to provide H^+(aq) through dissociation. The other way is the direct reduction of H_2CO_3(aq) and H_2S(aq).[40,49] The Tafel slopes for HER with H^+(aq), H_2CO_3(aq), and H_2S(aq) were frequently reported to be around –0.120 V/decade in literature at 20°C to 30°C, which is often used in modeling calculation.[14,38-39,45-46] Despite the differences in the species involved, these proposed reactions all had Tafel slope equations identical to the V-H mechanism, i.e., 1e mechanism.

To compare with the collected cathodic Tafel slopes, β values for the V-H mechanism and the expected Tafel slope for the V-T mechanism were calculated. For the V-T mechanism, the b_c value for this experimental system was calculated to be –0.0275 V/decade, which was smaller than the measured b_c by a factor of 9 to 27 in Table 6. A two-electron cathodic mechanism is also included in Table 7 for comparison, and its Tafel slope was calculated using Equation (8):

$$b_c = -\frac{2.303RT}{2\beta F} \quad (8)$$

Although the corresponding β values for the V-H mechanism and the two-electron cathodic mechanism were within 0 to 1 as shown in Table 7, they were very close to 0, especially for the two-electron cathodic mechanism. The corresponding β values were so low that further study on more suitable explanations is needed.

Corrosion Modeling Results

The experimental results were compared with those calculated for each condition using the

TABLE 8

Experimental (exp) and Modeled (mdl) E_{corr} (V_{SHE}) and pH After 60 Hours

	S-135			UD-165		
Gas	E_{corr}–exp	E_{corr}–mdl	pH	E_{corr}–exp	E_{corr}–mdl	pH
CO_2	–0.353±0.001	–0.414	3.9	–0.332±0.001	–0.424	4.2
CO_2+H_2S	–0.348±0.006	–0.394	3.0	–0.337±0.004	–0.411	3.4
H_2S	–0.444±0.002	–0.476	5.4	–0.460±0.002	–0.476	5.5

commercial modeling software,[50-51] and the modeled CR results are also given in Table 5. The CR calculations were performed assuming a rotating disk of generic carbon steel (UNS G10100) in the test environments listed in Table 1 at 4°C and 10 MPa (7 MPa in the H_2S-only system). The Fe dissolution over 60 h was taken into account. Hydrodynamic effects were approximated as a rotating disk electrode (Ø10 mm) at 150 rpm.

Modeled and experimental CRs were in reasonable agreement in the unmixed cases for UD-165 and S-135. In the CO_2-only case, modeled CRs for UD-165 were within 2 SD of experimental values, and within a factor of 5 for S-135. In the H_2S-only case, for both UD-165 and S-135, the modeled CRs were within 2 SD of the electrochemically obtained values and within a factor of 2 from the mass loss samples.

Modeled CRs for the CO_2+H_2S case were significantly different from what was experimentally obtained. As the modeled CRs for the mixed condition were very close to the modeled CRs in the CO_2-only case, it is likely that the model put this mix ratio of CO_2:H_2S in the sweet corrosion regime. These results suggest that the CR models should adjust their assumptions on the transition point between sweet and sour corrosion.

Table 8 shows a comparison between the experimentally measured E_{corr} and those calculated using the commercial modeling software after 60 h. Unlike the CR, the measured E_{corr} strongly correlated with the presence of CO_2 rather than H_2S. This suggests that E_{corr} was more of a function of pH, which is also given in Table 8. pH affects the equilibrium potential for the cathodic reactions (HERs), which in turn shifts E_{corr} to a more positive value when the pH is lower. pH also affects the equilibrium potential for the anodic reaction by changing the solubility of corrosion products in the aqueous phase. The modeled E_{corr} values followed a similar trend with the experimental values, and were within –90 mV from the experimental E_{corr}.

Pourbaix Diagrams and Surface Analysis

Pourbaix diagrams were generated using the commercial modeling software to predict the thermodynamically predominant corrosion products in the three gas conditions, which are depicted in Figures 7 through 9, respectively. The dissolved Fe after 60 h was used for the calculation, as shown in the figure captions. For the CO_2-only and CO_2+H_2S conditions, soluble Fe^{2+}(aq) and $FeHCO_3^+$(aq) were predicted to be the thermodynamically favorable products, which supports the assumption of active corrosion. For the H_2S-only condition, solid FeS(s) was predicted to be thermodynamically stable after 60 h. The FeS phase is pyrrhotite in the Pourbaix diagram because it is more thermodynamically stable and more protective than mackinawite, despite the formation of mackinawite at the early stage.[52] This suggests that the protective FeS(s) on the steel surface decreased the corrosion in the presence of H_2S. It agrees with the protective sulfide thin film reported in literature.[19,33] At the surface, the pH

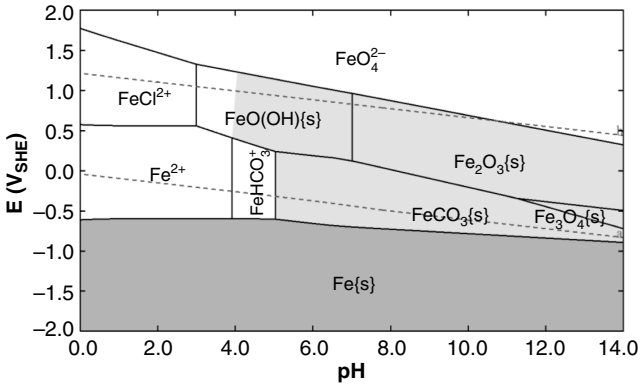

FIGURE 7. *Pourbaix diagram of Fe-H_2O-CO_2 system. Condition inputs: 4°C, 10 MPa, 0.9 mol/kg NaCl, 14.49 mol H_2O, 4.52 mol CO_2, 2.79×10^{-3} mol Fe. pH = 4.2 for UD-165 after 60 h.*

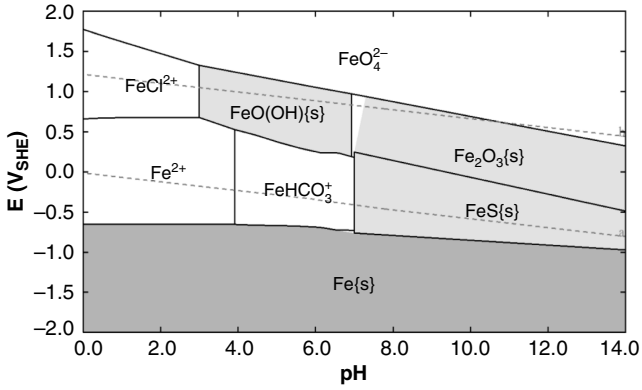

FIGURE 8. *Pourbaix diagram of Fe-H_2O-CO_2-H_2S system. Condition inputs: 4°C, 10 MPa, 0.9 mol/kg NaCl, 14.40 mol H_2O, 4.49 mol CO_2, 4.49×10^{-3} mol H_2S, 0.0404 mol Ar, 2.94×10^{-4} mol Fe. pH = 3.4 for UD-165 after 60 h.*

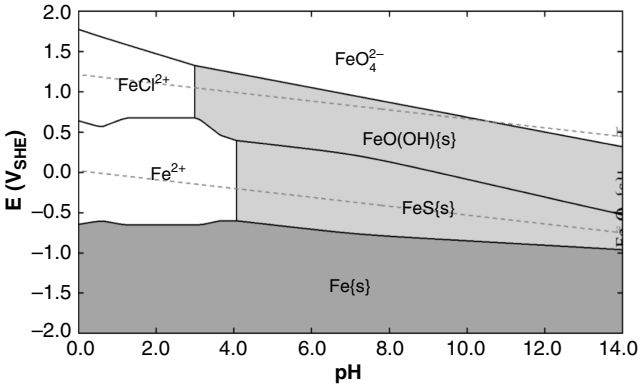

FIGURE 9. *Pourbaix diagram of Fe-H_2O-H_2S system. Condition inputs: 4°C, 7 MPa, 0.9 mol/kg NaCl, 20.20 mol H_2O, 6.30×10^{-3} mol H_2S, 0.5597 mol Ar, 1.30×10^{-4} mol Fe. pH = 5.5 for UD-165 after 60 h.*

and Fe^{2+}(aq) concentration were higher than in the bulk solution,[17] so the formation of $FeCO_3$(s) and FeS(s) were also likely at the surface in the CO_2-only and CO_2+H_2S cases, respectively. The lower CR in the CO_2+H_2S case indicates that the FeS(s) layer was more protective than $FeCO_3$(s).

Efforts were made to analyze the corroded surfaces using SEM and EDS. However, for all of the samples, the corrosion products on the surfaces noticeably changed color within 10 min of exposure to the atmosphere. The EDS analysis showed that the chemical composition over the surface was close to 1Fe:2O or 2Fe:3O.[53] The discoloration and the significant portion of oxygen on the sample surfaces suggested oxidation of the existing corrosion products after the samples were exposed to the atmosphere.

CONCLUSIONS

❖ Experimental results for two drill steels, S-135 and UD-165, showed a distinct drop in corrosion rate by more than one order of magnitude when transitioning from sweet to sour corrosion in 5 wt% NaCl solutions at 4°C and 7 MPa to 10 MPa total pressure. A CO_2:H_2S molar ratio as high as 1,000 was still enough for sour corrosion to dominate in the conditions tested. The corrosion rates in the CO_2-only condition were of the order of 0.5 mm/y to 2 mm/y, whereas the H_2S-only and CO_2+H_2S conditions gave corrosion rates of the order of 0.05 mm/y.

❖ The molar ratio of CO_2:H_2S = 1,000:1 in the whole system resulted in an aqueous CO_2(aq):H_2S(aq) ratio of approximately 440. Although the pH increased with the Fe dissolution, the dominant carbonate and sulfide species remained to be CO_2(aq) and H_2S(aq). The reaction mechanism was determined by the presence of H_2S, although its concentration was much lower than CO_2. This impact of a small amount of H_2S on the corrosion mechanism could be attributed to the specific adsorption of H_2S on the steel surface. Tafel analyses showed that the Bockris mechanism was unlikely for anodic reactions in the tested conditions.

❖ Good agreement was seen between the experimental and modeled corrosion rates in the CO_2-only and H_2S-only conditions. However, different from the experimental result, the modeling predicted the mixed case to be in the sweet corrosion regime. While the experimental corrosion behavior was strongly dependent on the presence of H_2S, both experimental and modeled E_{corr} values were related to the CO_2 content and pH.

❖ According to the Pourbaix diagrams, solid FeS(s) was predicted to be thermodynamically stable after 60 h in the H_2S-only condition. The protective FeS(s) thin film on the steel surface decreased the corrosion in the presence of H_2S.

DISCLAIMER

This report was prepared as an account of work sponsored by an agency of the United States Government. Neither the United States Government nor any agency thereof, nor any of their employees, makes any warranty, express or implied, or assumes any legal liability or responsibility for the accuracy, completeness, or usefulness of any information, apparatus, product, or process disclosed, or represents that its use would not infringe privately owned rights. Reference herein to any specific commercial product, process, or service by trade name, trademark, manufacturer, or otherwise does not necessarily constitute or imply its endorsement, recommendation, or favoring by the United States Government or any agency thereof. The views and opinions of authors expressed herein do not necessarily state or reflect those of the United States Government or any agency thereof.

ACKNOWLEDGMENTS

This work was completed as part of National Energy Technology Laboratory (NETL) research for the Department of Energy's Complementary Research Program under Section 999 of the Energy Policy Act of 2005. The authors would like to acknowledge OLI systems Inc. for providing access to OLI Analyzer modeling software and, especially, Dr. Andre Anderko for his helpful suggestions on modeling. The authors wish to acknowledge Roy Long (NETL Strategic Center for Natural Gas and Oil), Dr. Kelly Rose and Dr. Jeffrey Hawk (NETL Research and Innovation Center) for programmatic direction and technical support. We thank Dr. Winston Revie and two anonymous reviewers for their insightful and helpful comments.

REFERENCES

1. B.J. Berkowitz, H.H. Horowitz, *J. Electrochem. Soc.* 129 (1982): p. 468-474.

2. R. Feng, J. Beck, M. Ziomek-Moroz, S.N. Lvov, *Electrochim. Acta* 212 (2016): p. 998-1009.
3. E.C. Greco, W.B. Wright, *Corrosion* 18 (1962): p. 119t-124t.
4. Z.Y. Liu, X.Z. Wang, R.K. Liu, C.W. Du, X.G. Li, *J. Mater. Eng. Perform.* 23 (2014): p. 1279-1287.
5. G. Fierro, G.M. Ingo, F. Mancia, *Corrosion* 45 (1989): p. 814-823.
6. S.N. Smith, M.W. Joosten, "Corrosion of Carbon Steel By H_2S in CO_2 Containing Oilfield Environments," CORROSION 2006, paper no. 115 (Houston, TX: NACE International, 2006).
7. G.A. Zhang, Y. Zeng, X.P. Guo, F. Jiang, D.Y. Shi, Z.Y. Chen, *Corros. Sci.* 65 (2012): p. 37-47.
8. Y. Zheng, J. Ning, B. Brown, S. Nesic, *Corrosion* 71 (2015): p. 316-325.
9. M. Ziomek-Moroz, *J. Mater. Eng. Perform.* 21 (2011): p. 1061-1069.
10. W. Sun, S. Nešić, S. Papavinasam, *Corrosion* 64 (2008): p. 586-599.
11. J. Han, J. Zhang, J.W. Carey, *Int. J. Greenh. Gas Control* 5 (2011): p. 1680-1683.
12. K. Videm, A.M. Koren, *Corrosion* 49 (1993): p. 746-754.
13. F. Pessu, R. Barker, A. Neville, *Corrosion* 72 (2016): p. 78-94.
14. S. Nesic, J. Postlethwaite, S. Olsen, *Corrosion* 52 (1996): p. 280-294.
15. E. Abelev, T.A. Ramanarayanan, S.L. Bernasek, *J. Electrochem. Soc.* 156 (2009): p. C331-C339.
16. E. Abelev, J. Sellberg, T.A. Ramanarayanan, S.L. Bernasek, *J. Mater. Sci.* 44 (2009): p. 6167-6181.
17. Y.S. Choi, S. Nesic, S. Ling, *Electrochim. Acta* 56 (2011): p. 1752-1760.
18. M. Singer, B. Brown, A. Camacho, S. Nesic, *Corrosion* 67 (2011): p. 015004-1 to 015004-16.
19. K. Videm, J. Kvarekvål, *Corrosion* 51 (1995): p. 260-269.
20. NACE Standard SP0110-2010, "Wet Gas Internal Corrosion Direct Assessment Methodology for Pipelines" (Houston, TX: NACE, 2010).
21. S.N. Smith, "Discussion of the History and Relevance of the CO_2/H_2S Ratio," CORROSION 2011, paper no. 065 (Houston, TX: NACE, 2011).
22. A. Bishop, C. Bremner, A. Laake, C. Strobbia, P. Parno, G. Utskot, *Oilf. Rev.* 22 (2011): p. 36-49.
23. L.D. Perrigo, "An Overview of Corrosion in Cold Climates," CORROSION 2001, paper no. 306 (Houston, TX: NACE, 2001).
24. D.R. Lide, *CRC Handbook of Chemistry and Physics*, 84th ed. (Boca Raton, FL: CRC Press, 2003), p. 6-53.
25. Y. Zhang, *Environ. Sci. Technol.* 39 (2005): p. 7719-7724.
26. Q. Sun, H. Tian, Z. Li, X. Guo, A. Liu, L. Yang, *Fluid Phase Equilib.* 409 (2016): p. 131-135.
27. K.A. Rozman, "Corrosion and Fatigue of Oil Well Drilling Steels" (Master's thesis, Oregon State University, 2011), p. 46-50.
28. K.S. Pitzer, J.C. Pelper, R.H. Busey, *J. Phys. Chem. Ref. Data*, 13 (1984): p. 1-102.
29. R.A. Robie, B.S. Hemingway, J.R. Fisher, *U.S. Geol. Surv. Bull.* 1452 (1978): p. 12-24.
30. S.N. Lvov, *Introduction to Electrochemical Science and Engineering*, 1st ed. (Boca Raton, FL: CRC Press, 2015), p. 196-232.
31. ASTM G1-03, "Standard Practice for Preparing Cleaning and Evaluating Corrosion Test Specimens" (West Conshohocken, PA: ASTM International, 2003).
32. P. Wang, A. Anderko, R.D. Young, *Fluid Phase Equilib.* 203 (2002): p. 141-176.
33. K.J. Lee, S. Nesic, "The Effect of Trace Amount of H_2S on CO_2 Corrosion Investigated by Using the EIS Technique," CORROSION 2005, paper no. 630 (Houston, TX: NACE, 2005).
34. M. Stern, *Corrosion* 14 (1958): p. 60-64.
35. S. Nesic, N. Thevenot, J.L. Crolet, D.M. Drazic, "Electrochemical Properties of Iron Dissolution in the Presence of CO_2-Basics Revisited," CORROSION 1996, paper no. 003 (Houston, TX: NACE, 1996).
36. J. Tang, Y. Shao, J. Guo, T. Zhang, G. Meng, F. Wang, *Corros. Sci.* 52 (2010): p. 2050-2058.
37. F. Pessu, R. Barker, A. Neville, *Corrosion* 71 (2015): p. 1452-1466.
38. Y. Zheng, B. Brown, S. Nešić, *Corrosion* 70 (2014): p. 351-365.
39. Z.A. Iofa, V.V. Batrakov, Cho-Ngok-Ba, *Electrochim. Acta* 9 (1964): p. 1645-1653.
40. D.W. Shoesmith, P. Taylor, M.G. Bailey, D.G. Owen, *J. Electrochem. Soc.* 127 (1980): p. 1007-1015.
41. H. Ma, X. Cheng, G. Li, S. Chen, Z. Quan, S. Zhao, L. Niu, *Corros. Sci.* 42 (2000): p. 1669-1683.
42. J.O. Bockris, D. Drazic, A.R. Despic, *Electrochim. Acta* 4 (1961): p. 325-361.
43. M. Nordsveen, S. Nesic, R. Nyborg, A. Stangeland, *Corrosion* 59 (2003): p. 443-456.
44. G.A. Zhang, Y.F. Cheng, *Corros. Sci.* 51 (2009): p. 87-94.
45. D.R. Morris, L.P. Sampaleanu, D.N. Veysey, *J. Electrochem. Soc.* 127 (1980): p. 1228-1235.
46. X.L. Cheng, H.Y. Ma, J.P. Zhang, X. Chen, S.H. Chen, H.Q. Yang, *Corrosion* 54 (1998): p. 369-376.
47. R. Guidelli, R.G. Compton, J.M. Feliu, E. Gileadi, J. Lipkowski, W. Schmickler, S. Trasatti, *Int. Union Pure Appl. Chem.* 86 (2014): p. 259-262.
48. D. Landolt, *Corrosion and Surface Chemistry of Metals*, 1st ed. (Lausanne, Switzerland: EPFL Press, 2007), p. 180-191.
49. G.I. Ogundele, W.E. White, *Corrosion* 42 (1986): p. 71-78.
50. A. Anderko, P. McKenzie, R.D. Young, *Corrosion* 57 (2001): p. 202-211.
51. A. Anderko, R.D. Young, "Simulation of CO_2/H_2S Corrosion Using Thermodynamic and Electrochemical Models," CORROSION 1999, paper no. 031 (Houston, TX: NACE, 1999).
52. J.B. Sardisco, W.B. Wright, E.C. Greco, *Corrosion* 19 (1963): p. 354t-359t.
53. R. Feng, J. Beck, D. Hall, A. Buyuksagis, S.N. Lvov, M. Ziomek-Moroz, "Effects of CO_2 and H_2S on Corrosion of Martensitic Steels in NaCl at Low Temperature," CORROSION 2016, paper no. 7659 (Houston, TX: NACE, 2016).